

# An experimental study of the rearrangements of valence protons and neutrons amongst single-particle orbits during double $\beta$ decay in $^{100}\text{Mo}$ .

S. J. Freeman,<sup>1,\*</sup> D. K. Sharp,<sup>1</sup> S. A. McAllister,<sup>1</sup> B. P. Kay,<sup>2,†</sup> C. M. Deibel,<sup>3,4,‡</sup> T. Faestermann,<sup>5,6</sup> R. Hertenberger,<sup>6,7</sup> A. J. Mitchell,<sup>1,§</sup> J. P. Schiffer,<sup>3</sup> S. V. Szewc,<sup>1</sup> J. S. Thomas,<sup>1</sup> and H.-F. Wirth<sup>6,7</sup>

<sup>1</sup>*School of Physics and Astronomy, The University of Manchester, Manchester, M13 9PL, United Kingdom*

<sup>2</sup>*Department of Physics, University of York, York, YO10 5DD, United Kingdom*

<sup>3</sup>*Argonne National Laboratory, Physics Division, Argonne, Illinois 60439, USA*

<sup>4</sup>*Joint Institute for Nuclear Astrophysics, Michigan State University, East Lansing, Michigan 48824, USA*

<sup>5</sup>*Physik Department E12, Technische Universität München, D-85748 Garching, Germany*

<sup>6</sup>*Maier-Leibnitz Laboratorium der Münchner Universitäten (MML), D-85748 Garching, Germany*

<sup>7</sup>*Fakultät für Physik, Ludwig-Maximilians Universität München, D-85748 Garching, Germany*

(Dated: October 31, 2017)

The rearrangements of protons and neutrons amongst the valence single-particle orbitals during double  $\beta$  decay of  $^{100}\text{Mo}$  have been determined by measuring cross sections in  $(d,p)$ ,  $(p,d)$ ,  $(^3\text{He},\alpha)$  and  $(^3\text{He},d)$  reactions on  $^{98,100}\text{Mo}$  and  $^{100,102}\text{Ru}$  targets. The deduced nucleon occupancies reveal significant discrepancies when compared with theoretical calculations; the same calculations have previously been used to determine the nuclear matrix element associated with the decay probability of double  $\beta$  decay of the  $^{100}\text{Mo}$  system.

## I. INTRODUCTION

Over the past decade observations of neutrino flavor oscillations have provided fundamental information about the relative masses of neutrinos and mixing angles. However, the process of neutrinoless double  $\beta$  ( $0\nu 2\beta$ ) decay, if it is ever observed, would establish that the neutrino is a Majorana fermion and could be a way of obtaining the absolute scale for neutrino mass eigenstates. During such a decay, two neutrons in the ground state of an even-even nucleus transform into protons, usually in the ground-state of the final nucleus, with the simultaneous emission of two electrons. The rate of decay can be expressed as a product of three independent factors (see for example, Ref. [1]):

$$\frac{1}{T_{1/2}^{0\nu}} = G_{0\nu} |M_{0\nu}|^2 \langle m_{\beta\beta} \rangle^2.$$

Here,  $G_{0\nu}$  is the so-called phase-space factor and the information on the absolute mass scale appears via the term  $\langle m_{\beta\beta} \rangle$ , which is the effective neutrino mass in the simplest theoretical decay mechanisms. The dependence on nuclear structure is held in the nuclear matrix element  $M_{0\nu}$  that encapsulates the connection between initial and final nuclear states.

Both the nuclear matrix element and phase space factor are required if the absolute neutrino mass scale is

to be deduced from a future half-life measurement of neutrinoless double  $\beta$  decay. Indeed, estimates of these quantities are also critical in planning projects that set out to search for the decay process; the extremely low expected decay probabilities corresponding to  $T_{1/2}^{0\nu} \gtrsim 10^{25}$  yr require extremely large-scale, low-background source-detector systems.

Methods used in the calculation of phase-space factors are relatively well refined (see for example, Ref. [2] and references therein). However, there are significant difficulties associated with obtaining values of the nuclear matrix elements. Firstly, there are no other nuclear processes that directly probe the same matrix element, besides  $0\nu 2\beta$  decay itself. Secondly, even in a future era where  $0\nu 2\beta$  decay may have been unambiguously observed, it is unlikely that systematic phenomenological methods, which are common approaches to developing an understanding of many other complex nuclear characteristics, will be able to be applied in this case. The scale of investment required in attempts to observe a process with such low expected decay probabilities is such that, even if  $0\nu 2\beta$  decay is eventually observed, we are unlikely to have data on more than one or two isotopes for a considerable period of time, making phenomenology difficult. Therefore, in order to proceed, robust theoretical calculations of the nuclear matrix elements must be developed.

There has been significant progress in the understanding of the theoretical calculation of nuclear matrix elements for  $0\nu 2\beta$  decay over the last decade. As an illustration, in 2004, a provocative article [3] suggested that the variation in the size of matrix elements calculated in different ways could be as much as two orders of magnitude. Whilst more recent developments have reduced the variation somewhat (see for example Ref. [1]), the convergence of different theoretical approaches in itself is no guarantee that they are correct. It is also important

\* Correspondence to: [sean.freeman@manchester.ac.uk](mailto:sean.freeman@manchester.ac.uk)

† Current address: Argonne National Laboratory, Physics Division, Argonne, Illinois 60439, USA

‡ Current address: Department of Physics and Astronomy, Louisiana State University, Baton Rouge, LA 70803, USA.

§ Current address: Department of Nuclear Physics, Research School of Physics and Engineering, The Australian National University, Canberra, ACT 2601, Australia.

to bear in mind that the matrix element appears as a square in the decay probability, increasing the variation between different models in their predictions of observable quantities.

One way forward is to determine which accessible properties of nuclei are most directly relevant to the matrix elements. These properties can then be measured and the results used to gauge to what extent they can be reproduced by the models used to calculate the matrix elements. In this way, the calculational frameworks adopted can be constrained by comparison with other pertinent nuclear observables.

Double  $\beta$  decay involves the decay of two neutrons into two protons within a nuclear system. The simplest of several mechanisms proposed involves a pair of virtual neutrinos as the nucleons transform. If neutrinos are Majorana in nature, the annihilation of the virtual neutrinos leads to the neutrinoless version of the decay. The whole process is often viewed as proceeding via the excitation of states in the intermediate isobaric nucleus between the parent and daughter (see, for example, [1] for more details). The short distance scales within the nuclear system imply the involvement of large virtual momenta (up to  $\sim 100$  MeV/c), leading to high virtual excitation energies (50-100 MeV) in the intermediate system and angular momenta up to  $\sim 7 - 8\hbar$ . Unlike the two-neutrino form of double beta decay, which proceeds via a small number of virtual  $1^+$  states at relatively low excitation, neutrinoless double  $\beta$  decay involves a large number of states to high excitation. It therefore seems unlikely that neutrinoless double  $\beta$  decay exhibits strong sensitivity to the detailed structure of the intermediate nucleus. However, the ground states of the initial and final nuclei must play a role in determining the value of the matrix element. If there are significant rearrangements of other nucleons, beyond the simple conversion of the two neutrons into protons, the decay rates may be diminished; a change in nuclear deformation accompanying the decay is an extreme example of such a rearrangement. Such inhibition is common in other types of nuclear processes. The differences in the occupation of the valence single-particle states before and after the decay characterises such rearrangements, which are likely to have important consequences for the matrix element.

Determining the valence populations of neutrons and protons, and the difference in these populations between initial and final states, addresses a critical ingredient of the overlap that determines the matrix elements [4]. For example, we carried out systematic measurements of the valence proton and neutron occupancies in  $^{76}\text{Ge}$  and  $^{76}\text{Se}$ , a potential  $0\nu 2\beta$  parent-daughter system [5, 6]. Several authors have revisited theoretical predictions in the light of this data, leading to a reduction in the difference between predictions of the matrix elements based on the quasi-particle random phase approximation (QRPA) compared to those made using the interacting shell model (as examples, Refs. [7] and [8]). Several measurements have been made to characterise other systems and pro-

vide further benchmarks for theoretical approaches [9–11].

Here we report on a consistent set of single-nucleon transfer experiments that have been used to determine the valence nucleon occupancies for  $^{100}\text{Mo}$  and  $^{100}\text{Ru}$ . This builds on our previous experimental study [12] of the validity of the BCS approximation in these nuclei, which is a basic assumption of the widely used QRPA method. Nucleon occupancies in  $^{98}\text{Mo}$  and  $^{102}\text{Ru}$  were also measured and used as consistency checks.  $^{100}\text{Mo}$  and  $^{100}\text{Ru}$  are parent and daughter for a potential  $0\nu 2\beta$  decay whose  $Q$  value makes it a good candidate in which to observe the process [1]. There are several experiments that propose searches for double  $\beta$  decay of  $^{100}\text{Mo}$ . For example, it is one of the isotopes that may be used in the SuperNEMO  $0\nu 2\beta$  decay experiment and was a source in the predecessor NEMO-3 [13, 14]. Other examples include the AMoRE [15] and CUPID/LUMINEU [16] experiments which have proposed plans to use a cryogenic scintillation detector based on molybdate crystals.

This potential double- $\beta$ -decay system lies toward the edge of an interesting region of the chart of nuclides. Nuclei with  $Z \sim 40$  exhibit a sudden onset of deformation resulting in a dramatic shape change from spherical to prolate shapes near  $N = 60$ . The first indication of this transition came from early studies of  $\gamma$  emission from spontaneous fission fragments [17], measurements that have since been refined significantly with the improvements in detection technology (see for example [18]). For molybdenum and ruthenium isotopes, the evolution in shape persists, but is more gradual in nature. For example, a smoother shape transition has recently been inferred in mean-square charge radii of molybdenum fission fragments [19] from  $A \sim 98$  to 104 using laser spectroscopy of separated singly-charged ions. Classical optical spectroscopy of enriched isotopes of ruthenium [20] paints a similar picture, although there is some evidence for triaxial shapes in ruthenium fission fragments beyond  $N = 60$  [21]. The transitional nature of  $^{100}\text{Mo}$  is also clear from pair transfer studies. For example, our recent  $(p,t)$  reaction studies on targets of  $^{98,100}\text{Mo}$  and  $^{100,102}\text{Ru}$  [12] found that 95% of the neutron pair transfer strength to  $0^+$  states is contained in the ground-state transition, except for the reaction leading to  $^{98}\text{Mo}$ , where a state at 735 keV was populated with  $\sim 20\%$  of the ground-state transition strength. This transitional nature, and potential structural differences between parent and daughter, are likely to present challenges for the calculations of the associated  $0\nu 2\beta$  decay matrix elements.

Over many years, data has been accumulated on single-nucleon transfer data that might yield the occupancies required to constrain calculations of the  $0\nu 2\beta$  matrix elements. Molybdenum isotopes have been studied in neutron transfer experiments. There are several published studies of the  $(d,p)$  and  $(p,d)$  reactions on  $^{100}\text{Mo}$  [22–31]. Studies of both these reactions, albeit fewer in number, have been made on targets of  $^{98}\text{Mo}$  [27, 32–34] and  $^{102}\text{Ru}$  [35–39]. Neutron addition has been performed on

$^{100}\text{Ru}$  [40, 41], although the neutron removal with the  $(p, d)$  reaction has not. Of these four targets, only  $^{100}\text{Mo}$  has been studied in the  $(^3\text{He}, \alpha)$  reaction [42], which is required to provide good matching for large angular-momentum transfer. Where data does exist in the literature, the experiments were performed at different times using different experimental techniques, different bombarding energies, different ranges of excitation energy and so on. Reaction modeling has been employed differently in each case, using a variety of computer codes and employing a host of different approximations and potential choices. In some cases, measured cross sections have not been published. As a result, the existing literature, whilst useful in establishing many spin-parity assignments to relevant states, has neither the overall precision nor the consistency required to determine the changes in neutron occupancies between parent and daughter in this potential  $0\nu 2\beta$  system.

With regards to proton transfer reactions,  $(^3\text{He}, d)$  studies have been made on  $^{98,100}\text{Mo}$  [43–45], but not on the relevant ruthenium isotopes. The majority of previous studies were done at significantly worse resolution than the current work; resolution was one of the contributory factors in determining how high in excitation energy measurements could be undertaken. The comments above concerning the consistency of experimental approach and reaction modeling are also pertinent for the proton transfer data in the literature.

In the current work, several transfer reactions have been employed. The  $(p, d)$  and  $(d, p)$  reactions were used to gain spectroscopic information on the low- $\ell$  valence neutron states. In these reactions, we have determined the normalization of the necessary reaction model calculations by requiring the sums of strength for addition and removal to be equal to the total degeneracy of the relevant orbits. The  $(^3\text{He}, \alpha)$  reaction was used to measure high- $\ell$  states, with a reaction normalization determined by the requirement that the sum of associated high- $\ell$  strength and the normalized low- $\ell$  strength from the  $(p, d)$  reactions yields the expected number of valence neutrons. Using these reaction normalizations, neutron occupancies are deduced from the neutron-removing reactions for the  $0g_{7/2}$ ,  $1d$ ,  $2s_{1/2}$  and  $0h_{11/2}$  orbitals.

For protons, the  $(^3\text{He}, d)$  reaction was used to determine proton vacancies. This reaction is reasonably well matched for all the valence orbitals of interest and was therefore normalized by requiring the total extracted transfer strengths to sum to the total number of valence proton holes. Orbital vacancies were then deduced for the proton  $0g_{9/2}$ ,  $1p$  and  $0f_{5/2}$  orbitals.

This current publication is organised in the following way. Common aspects of the experimental methodology will be discussed first. The features of the neutron and proton transfer reaction experiments will be considered in separate sections covering specific features of the results and analysis, the spin-parities of the populated states and features of the transfer strength distributions. The approach used to normalize the reaction modeling for the

transfer of both types of nucleon will be described followed by a discussion of the extracted occupancies and their uncertainties. The deduced proton and neutron occupancies will finally be compared to those used in theoretical calculations of the double  $\beta$  decay matrix elements and some conclusions are reached. For the sake of brevity, the detailed experimental data is available as Supplemental Material [46] and discussion here will concentrate on more global information such as summed strengths.

## II. EXPERIMENTAL METHODS

Beams of the required ions were delivered by the MP tandem accelerator at the Maier-Leibnitz Laboratorium of the Ludwig-Maximilians Universität and the Technische Universität München. They were used to bombard isotopically enriched targets of  $^{100}\text{Mo}$  (97.39%),  $^{100}\text{Ru}$  (96.95%),  $^{98}\text{Mo}$  (97.18%) and  $^{102}\text{Ru}$  (99.38%) with nominal thicknesses of  $100 \mu\text{g}/\text{cm}^2$ , which were evaporated onto thin carbon foils with thicknesses in the range of 8–20  $\mu\text{g}/\text{cm}^2$ . Beam currents were measured using a Faraday cup behind the target ladder connected to a current integrator and were typically between 500 and 700 nA.

Light reaction products were momentum analyzed using a Q3D magnetic spectrometer [47]. The spectrometer entrance aperture, which defines the solid-angle acceptance of the system, was set at a nominal value of 13.9 msr throughout the entire experiment to minimize systematic uncertainties. At the focal plane of the spectrometer, a multi-wire gas proportional counter backed by a plastic scintillator was used to measure position, energy loss and residual energy of the ions passing through it [48]. The focal-plane position was determined by reading out 255 cathode pads, positioned every 3.5mm across the counter. Each pad was equipped with an individual integrated preamplifier and shaper. Events were registered when three to seven adjacent pads had signals above threshold. The digitized signals on active pads were then fitted with a Gaussian line shape resulting in a position measurement with a resolution that was better than 0.1 mm. Outgoing particles were identified by a combination of their magnetic rigidity and their energy-loss characteristics in the proportional counter and scintillator.

In order to extract absolute cross sections, the product of the target thickness and the solid angle of the spectrometer entrance aperture was determined using Coulomb elastic scattering. The data were collected in two distinct running periods and elastic scattering was performed separately for both. In the first run, elastic scattering of 12-MeV  $^3\text{He}$  ions at  $\theta_{\text{lab}}=25^\circ$  was used and in the second, similar measurements with 9-MeV deuterons at  $\theta_{\text{lab}}=12^\circ$ . The elastic scattering cross sections under these conditions are predicted to be within 2% and 4% of the Rutherford scattering formula, respectively, according to optical-model calculations performed with the potentials discussed below. Lower beam cur-

rents were used for the elastic-scattering measurements compared to the transfer reactions, requiring a different scale on the current integrator. The calibrations of all the scales used during the experiment were determined using a calibrated current source to ensure that relative values are well known. Consistent results were obtained from the two different running periods and the overall uncertainty in the cross sections deduced using this approach was estimated to be around 5%.

Reaction modeling must be performed to extract spectroscopic strengths from the measured cross section and the associated calculations were performed using the distorted-wave Born approximation (DWBA). The approximations involved are best met at the first maximum of the angular distribution of transfer products. In order to extract robust spectroscopic factors, data were therefore taken at the angles corresponding to these maxima for the relevant  $\ell$  transfers in each reaction. Measurements were also made at some other angles when time allowed. The angles where data were taken are summarised in Table I for each reaction. Although much of the measured strength was associated with states having pre-existing spin-parity assignments, the resulting sets of data map out angular distributions that were sufficient to discriminate between different angular momentum transfers to confirm or, where necessary, make  $\ell$  assignments. The comparison between the differently matched reactions,  $(p, d)$  and  $(^3\text{He}, \alpha)$ , helps to extend the range of momentum transfers investigated in the angular distributions and the differences in cross section assisted some of the  $\ell$  assignments, as discussed below.

Given the large number of cross section measurements made to states populated over a range of several MeV in excitation, in four different reactions at several angles and on four different targets, the state-by-state cross section data is given in the Supplemental Material [46].

### A. Neutron Transfer Reactions

The neutron-removal reactions,  $(^3\text{He}, \alpha)$  and  $(p, d)$ , were carried out with beams of  $^3\text{He}$  ions at an energy of 36 MeV and protons at 24 MeV, respectively. The  $(d, p)$  neutron-adding reaction was also performed using a deuteron beam at 15 MeV. Data were recorded up to excitation energies of at least 3 MeV in each residual nucleus. For the  $(d, p)$  and  $(p, d)$  reactions, this was achieved using three different magnet settings, arranged so that the subsequent spectra overlapped in excitation by at least 100 keV. The lower dispersion associated with the magnet settings for the  $(^3\text{He}, \alpha)$  reaction enabled data to be recorded at one magnet setting. Figs. 1, 2 and 3 show typical energy spectra of outgoing ions from these reactions. The spectra were calibrated using previously observed strongly populated final states [49–52].

Excitation energies were estimated to be accurate to better than  $\sim 3$  keV for the  $(d, p)$  reaction and around  $\sim 2$  keV for the  $(p, d)$  reaction. For the  $(^3\text{He}, \alpha)$  reaction,

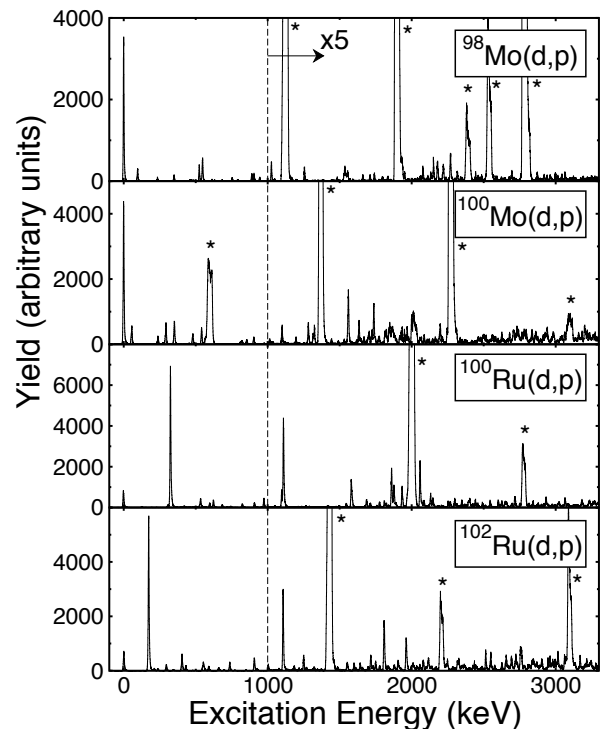


FIG. 1. Spectra of protons from the  $(d, p)$  reaction on targets of  $^{98}\text{Mo}$ ,  $^{100}\text{Mo}$ ,  $^{100}\text{Ru}$  and  $^{102}\text{Ru}$  at a laboratory angle of  $8^\circ$  as a function of the excitation energy in the residual nucleus. The portions of the spectra to the right of the dotted line have been scaled up by a factor of five. The broader peaks that appear in these spectra are reactions on light target contaminants, the strongest of which are marked by an asterisk.

low-lying states are accurate to  $\sim 5$  keV, rising to  $\sim 10$  keV at the higher excitation energies measured. Typical energy resolutions obtained were  $\sim 30$  keV FWHM for  $(^3\text{He}, \alpha)$  and  $\sim 8$  keV FWHM for  $(p, d)$  and  $(d, p)$  reactions.

Peaks corresponding to reactions on carbon and oxygen target contaminants are present in the  $(d, p)$  spectra with larger widths than those from the main target material due to their larger kinematic shift. These contaminant peaks obscured groups of interest at some angles, but the difference in their kinematic shifts meant that angles were always available where clean measurements could be made. The spectra were also checked carefully for the presence of any peaks arising from isotopic contaminants in the target material and these were excluded from subsequent analysis.

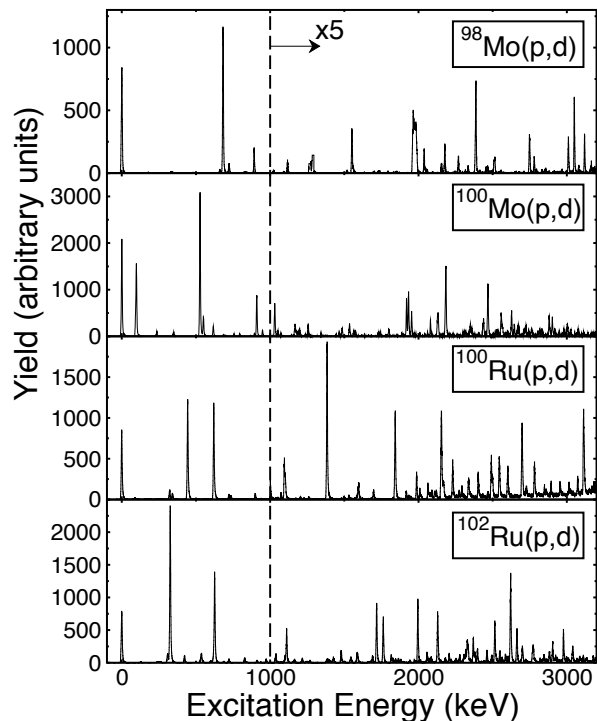


FIG. 2. Spectra of deuterons from the  $(p,d)$  reaction on targets of  $^{98}\text{Mo}$ ,  $^{100}\text{Mo}$ ,  $^{100}\text{Ru}$  and  $^{102}\text{Ru}$  at a laboratory angle of  $6^\circ$  as a function of the excitation energy in the residual nucleus. The portions of the spectra to the right of the dotted line have been scaled up by a factor of five.

TABLE I. List of laboratory angles at which measurements were made for each of the reactions used. Due to target problems, data were not measured for the  $^{98}\text{Mo}(^3\text{He},d)$  reaction at  $14^\circ$  and  $22^\circ$ .

Reaction	Laboratory Angles
$(p,d)$	$6^\circ, 18^\circ, 31^\circ, 40^\circ$
$(d,p)$	$8^\circ, 18^\circ, 27^\circ, 33^\circ$
$(^3\text{He},\alpha)$	$10^\circ, 15^\circ, 20^\circ, 25^\circ$
$(^3\text{He},d)$	$6^\circ, 10^\circ, 14^\circ, 18^\circ, 22^\circ$

The differences in the kinematic matching between the two different neutron-removal reactions are apparent in the spectra. For example, the  $\ell = 0$  ground state in  $^{99}\text{Mo}$  is clearly visible in the  $(p,d)$  spectrum (Fig. 2) with a cross section of 2.98 mb/sr. However, it is hardly discernible at all in Fig. 3, having a cross section of only 7  $\mu\text{b/sr}$  in the  $(^3\text{He},\alpha)$  reaction at  $10^\circ$ , and approaches the observation limit of around 1  $\mu\text{b/sr}$  at other angles.

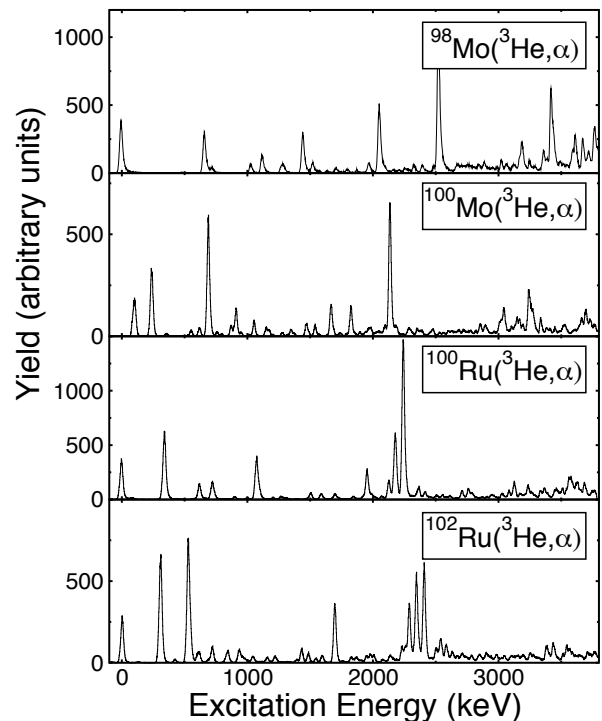


FIG. 3. Spectra of  $\alpha$  particles from the  $(^3\text{He},\alpha)$  reaction on targets of  $^{98}\text{Mo}$ ,  $^{100}\text{Mo}$ ,  $^{100}\text{Ru}$  and  $^{102}\text{Ru}$  at a laboratory angle of  $10^\circ$  as a function of the excitation energy in the residual nucleus.

The ground state is only visible at all due to the low level density in this region; other excited  $\ell = 0$  transitions in the  $(^3\text{He},\alpha)$  reaction are generally much weaker and obscured by stronger transitions.

For many of the states populated in the residual odd nuclei, angular-momentum quantum numbers have already been determined in a variety of previous studies that are summarized in Refs. [49–52]. Overall more than 85% of the transfer strength used in the sum-rule analysis from which the occupancies are extracted (as described below) is associated with states that have a previously determined assignment. Where new assignments were made or previous assignments checked, this was done on the basis of the angular distribution of the light reaction product and a comparison of the cross section between the differently matched neutron-removal reactions. Some examples of angular distributions are shown in Fig. 4 where the first maxima clearly appear at higher angles for higher  $\ell$  transfers, except for the mismatched  $(^3\text{He},\alpha)$  reaction where the forward-peaked shapes are less characteristic of the  $\ell$  transfer. The strategy adopted when making new assignments was to use the shape of the distributions from  $(p,d)$  and  $(d,p)$  reactions, but confirm any high- $\ell$  assignments using the comparison of the cross

sections from  $(p, d)$  and  $({}^3\text{He}, \alpha)$  reactions. Examples of the latter are shown in Fig. 5 where the ratio of these cross sections at forward angles for  $\ell = 4$  and  $\ell = 5$  transitions is plotted. The momentum matching was such that  $\ell = 5$  transitions are characterised by larger  $({}^3\text{He}, \alpha)$  to  $(p, d)$  cross section ratios than those with  $\ell = 4$ . Cross section ratios for transitions with  $\ell < 4$ , not shown in Fig. 5, are smaller by factors of ten compared with those plotted. Whilst most of the consideration of such ratios was done using data at  $6^\circ$  for the  $(p, d)$  reaction and  $10^\circ$  for the  $({}^3\text{He}, \alpha)$  reaction, ratios involving cross sections at other laboratory angles have similar features and were used where needed, as noted in the Supplemental Material [46]. This assignment methodology produced results that were consistent with previous assignments where they are available in the literature.

Most of the states with significant contributions to the sum-rule analysis discussed below have assignments from previous work. There are a few strong states where new assignments have been made here, most notably in the neutron-removal reactions on Mo targets populating states via  $\ell = 5$  transfer. Newly assigned states at 2.043 and 2.089 MeV in  ${}^{97}\text{Mo}$ , carry 59% and 7% of the measured  $\ell = 5$  strength respectively in that system. Similarly, two newly assigned states at 1.662 and 1.818 MeV in  ${}^{99}\text{Mo}$  contribute a third of the observed  $\ell = 5$  strength in  ${}^{101}\text{Mo}$ . These states have  $(p, d)$  cross sections that peak at the most backward angles studied and the ratios of  $({}^3\text{He}, \alpha)$  to  $(p, d)$  cross sections are large and consistent with other  $\ell = 5$  transitions. In the  $(d, p)$  reaction, around a third of the  $\ell = 2$  strength on each of the molybdenum targets was from states with new assignments. In the  $(p, d)$  reaction, the only significant newly assigned strength of relevance to the later analysis was the addition of new  $\ell = 0$  strength in  ${}^{99}\text{Ru}$ . Much of this newly assigned low- $\ell$  strength arises from extending the excitation-energy range over which measurements have been made; for example, states populated in  $(d, p)$  reactions on molybdenum targets are only reported to around 1.5 MeV in the literature [49, 51]. For some weaker newly observed transitions, only tentative assignments were possible, but the contribution of these to the overall sum-rule analysis is naturally very small.

It is instructive at this point to consider the distribution of transfer strength in the residual nuclei. Figs. 6 and 7 show the distributions of spectroscopic strength defined as the spectroscopic factor  $C^2S$  for removal reactions or  $(2j + 1)C^2S$  for addition reactions. (The spectroscopic factors have been obtained using the DWBA modeling and reaction normalization discussed in detail in Section III and are available as part of the Supplementary Material [46].)

Fig. 6 shows the distribution of spectroscopic strength for low  $\ell$  transfers obtained from the  $(d, p)$  and  $(p, d)$  reactions as a function of excitation energy, where strength associated with states populated in the latter reaction is plotted at negative excitation energies. Considering first the strength distributions for valence orbitals, the  $\ell = 0$

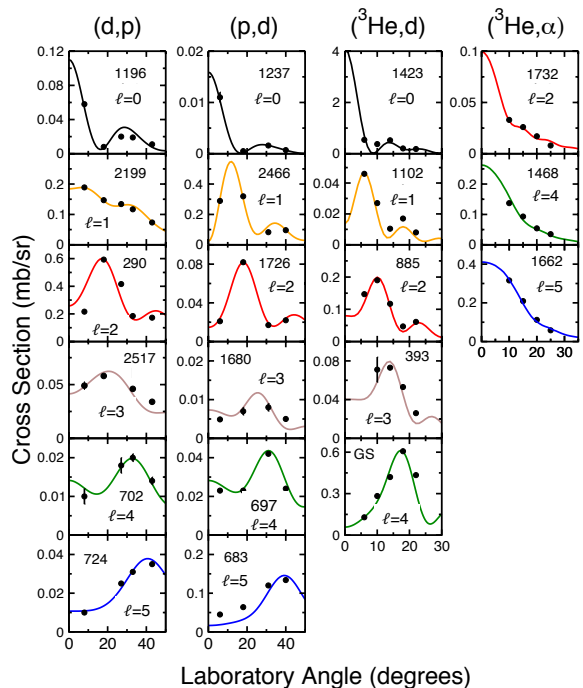


FIG. 4. (Color online) Examples of angular distributions for the  $(d, p)$ ,  $(p, d)$ ,  $({}^3\text{He}, d)$  and  $({}^3\text{He}, \alpha)$  reactions on a  ${}^{100}\text{Mo}$  target. An example of each  $\ell$  value is shown and compared to the results of DWBA calculations using parameters listed in Section III;  $\ell = 0$  (black),  $\ell = 1$  (orange),  $\ell = 2$  (red),  $\ell = 3$  (brown),  $\ell = 4$  (green) and  $\ell = 5$  (blue). Transitions with  $\ell = 0, 1$  and  $3$  were not strongly observed in the  $({}^3\text{He}, \alpha)$  reaction. The angular distributions are labelled with  $\ell$  value and the excitation energy in the residual system in units of keV.

distributions are approximately Lorentzian in form with a centroid close to zero and a width of around 100 keV. The  $\ell = 2$  strength is similarly centred at low excitation energies. Not all the states with  $\ell = 2$  have a firm  $J^\pi$  assignment in the literature, but many of the stronger states at low excitation do have information on the spin quantum numbers. For example, the strong states clustered around 0 MeV in Fig. 6 are  $5/2^+$  states. Most of the states with a strength greater than 0.5 at energies above 250 keV have  $3/2^+$  assignments, where  $J^\pi$  assignments are available. This is qualitatively consistent with the energetic ordering of the  $d_{5/2}$  and  $d_{3/2}$  orbitals. Rough estimates of the unobserved strength were obtained in the following way. Lorentzian curves were fitted to the data and the area under these fits outside of the excitation energy range of the measurements was only  $\sim 2$  to 3% of the total, suggesting that the majority of the low-lying strength of the  $s_{1/2}$  and  $d$  orbitals has been captured in the data. Such estimates are consistent with similar studies that have been performed [53].

The out-of-shell strength distributions are somewhat different in character and weaker in overall strength; note the difference in the scale of the vertical axes for Fig. 6

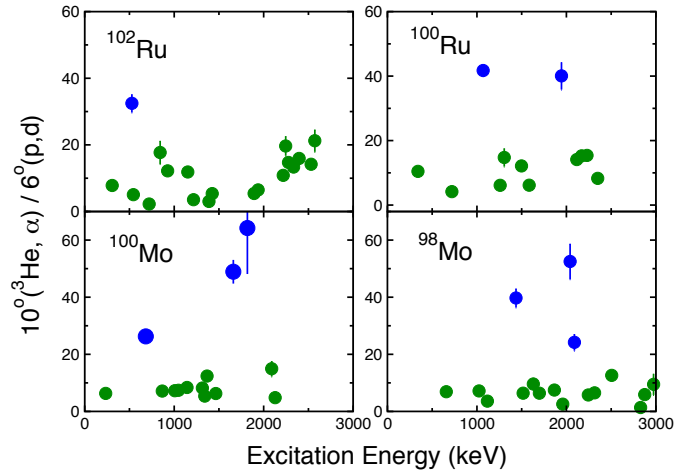


FIG. 5. (Color online) The ratio of the cross section leading to the population of states in the  $({}^3\text{He}, \alpha)$  reaction at a laboratory angle of  $10^\circ$  to that leading to the same states in the  $(p, d)$  reaction at  $6^\circ$  for  $\ell = 4$  (green) and  $\ell = 5$  (blue) transitions, plotted as a function of excitation energy in the residual nucleus. The plots are labeled by the target isotope.

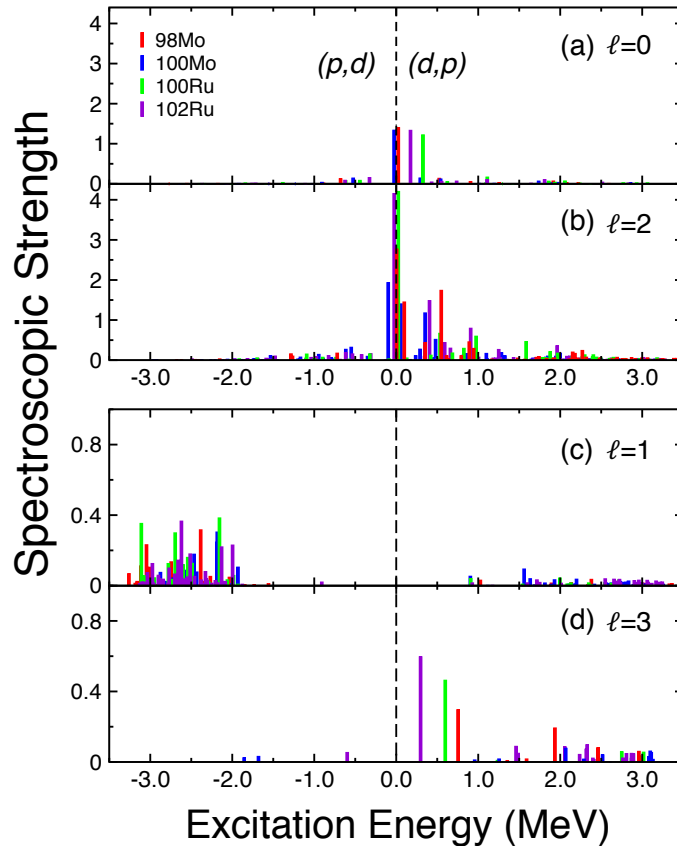


FIG. 6. (Color online) Distributions of the spectroscopic strength of states populated in  $(p, d)$  and  $(d, p)$  neutron transfer reactions on targets of  ${}^{102}\text{Ru}$  (violet),  ${}^{100}\text{Ru}$  (green),  ${}^{100}\text{Mo}$  (blue) and  ${}^{98}\text{Mo}$  (red) as a function of excitation energy for (a)  $\ell = 0$ , (b)  $\ell = 2$ , (c)  $\ell = 1$  and (d)  $\ell = 3$  transfers. Note the difference in the vertical scales of the strength distributions for the valence orbitals in (a) and (b) compared to those of the out-of-shell strengths in (c) and (d). For the purposes of the figure, strengths are plotted at negative energies for the  $(p, d)$  reaction and at positive energies for the  $(d, p)$  reaction. The strength of individual states has been obtained from the measured cross sections using the DWBA reaction modeling and normalization procedures described in Section III. For clarity, the strengths for the ground-state transitions in the two reactions have been combined and shifted slightly in excitation energy from zero.

(a) and (b) compared with Fig. 6 (c) and (d). The  $\ell = 1$  strength, shown in Fig. 6(c), appears at higher energies in both reactions, consistent with the tails of strength distributions from the next oscillator shells above and below the valence orbitals.

The  $\ell = 3$  strength (see Fig. 6(d)) is similarly weak and mostly at high excitation in the  $(d, p)$  reaction, constituting a tail of strength from the shell above. There are single low-lying states populated by the  $(d, p)$  reaction in  $^{99}\text{Mo}$ ,  $^{101}\text{Ru}$  and  $^{103}\text{Ru}$  with spectroscopic strengths up to  $\sim 0.6$ ; these states have also been observed in previous work, for example [37, 40, 55]. Low-lying  $\ell = 3$  strength of this magnitude, associated with the  $1f_{7/2}$  orbital from the shell above, has been predicted by modeling these transitional systems as a single neutron outside a weakly prolate core (see detailed discussion in Ref. [40] and references therein). In the  $(p, d)$  reaction,  $\ell = 3$  strength is limited to a small number of very weakly populated states lying below 2 MeV. No strength has been identified with  $^{100}\text{Ru}$  and  $^{98}\text{Mo}$  targets, a single state with spectroscopic strength of 0.05 in  $^{101}\text{Ru}$  and two rather tentative  $\ell = 3$  transitions in  $^{99}\text{Mo}$ , each with strength less than 0.01, have been found. These observations put a limit on the occupancy of  $1f$  orbitals in the ground states of the target nuclei. It appears that the occupancy of the  $1f$  orbital in these nuclei is  $\lesssim 0.05$  neutrons, while the  $0f$  shell is well below the Fermi surface.

Fig. 7 shows a similar plot of spectroscopic strength for higher  $\ell$  transfers taken from the  $(^3\text{He}, \alpha)$  reaction. The  $\ell = 5$  strength is confined to a small number of states at excitation energies in each residual nucleus at or below  $\sim 2$  MeV. The  $\ell = 4$  strength distribution is somewhat different with a number of strong states at low energy, then the strength falls with increasing excitation until some more prominent  $\ell = 4$  peaks are encountered above 2 MeV. This is consistent with an overall picture of low-lying  $\ell = 4$  strength associated with the valence  $g_{7/2}$  orbital, but the presence of the deeper lying  $g_{9/2}$  state at higher excitation. Indeed, below 2 MeV, all the states with spectroscopic strengths larger than 0.4 have been assigned as  $J^\pi = 7/2^+$  in the literature [49–51], although some weak  $9/2^+$  states are also present in the same energy region. States whose spins are known to be  $9/2^+$  are indicated by an asterisk in Fig. 7, although above 2 MeV the spins of most of the states are unknown. However, in  $^{97}\text{Mo}$ , the strong state at 2.510 MeV was assigned as  $J^\pi = 9/2^+$  from analysing powers measured in a  $(d, t)$  reaction [54]. The lack of a complete set of  $J^\pi$  assignments introduces some problems for the current work in disentangling  $g_{7/2}$  and  $g_{9/2}$  strengths. A choice was made to associate all  $\ell = 4$  strength below 2 MeV that does not have a previous  $J^\pi = 9/2^+$  assignment with the  $g_{7/2}$  orbital. Clearly other choices might be made in the absence of new spin assignments, which introduces a systematic error in the final occupancy analysis that will be discussed below. To place this choice on a more quantitative footing, more than 90% of the strength associated here with the  $g_{7/2}$  orbital is in states with existing  $7/2^+$

assignments.

## B. Proton Transfer Reactions

The  $(^3\text{He}, d)$  proton-adding reactions were initiated using beams at an energy of 36 MeV. Data were recorded up to excitation energies of at least 2.7 MeV, performed at one magnet setting. Excitation energies of states in the residual nucleus were obtained by comparison with previously observed states taken from Refs. [49–51] and some representative spectra are shown in Fig. 8. The excitation energies obtained were generally measured to better than 3 keV, although in the ruthenium targets this rises to 10 keV at the highest excitations measured as there are fewer previously known states for calibration. Typical energy resolutions of 20 keV FWHM were obtained and measurements were made at a series of angles listed in Table I.

The assignments of  $\ell$  transfer were checked using angular distributions and Fig. 4 shows some examples. There are no previously reported data for this reaction on ruthenium targets in the literature, although nearly all of the states carrying strength from the valence nucleon orbitals have assignments deduced by other types of measurement [49–51]. In total, 92% of the strength used in deducing the proton occupancies is associated with the population of states with previous assignments; across the individual targets used, the percentage of strength with previous assignments are 99%, 82%, 97% and 93% for  $^{98}\text{Mo}$ ,  $^{100}\text{Mo}$ ,  $^{100}\text{Ru}$  and  $^{102}\text{Ru}$ , respectively. In the reactions on  $^{100}\text{Mo}$ , the new assignments made here were predominantly  $\ell = 4$  states. Some examples of the relevant angular distributions are compared to that for the known  $\ell = 4$  ground-state transition and to DWBA predictions in Fig. 9.

The distributions of spectroscopic strength  $(2j+1)C^2S$  for proton addition obtained using the  $(^3\text{He}, d)$  reaction are shown in Fig. 10(a)–(e). The transfer associated with the proton valence orbitals has  $\ell = 1, 3$  and 4. With increasing excitation energy, the  $\ell = 1$  strength falls off rapidly and is contained mostly in the first 1.5 MeV as shown in Fig. 10(b). There is not much  $\ell = 3$  strength, all of which lies at energies below 1.1 MeV; no  $\ell = 3$  transitions were apparent in reactions on the  $^{98}\text{Mo}$  target. For  $\ell = 4$ , the majority of the strength identified in the  $(^3\text{He}, d)$  reaction is in a single low-lying  $9/2^+$  state below 0.5 MeV in each residual nucleus, with some weaker fragments at energies up to 1.5 MeV (see Fig. 10(e)).

The distributions of strength associated with non-valence orbitals with  $\ell = 0$  and 2 (see Fig. 10(a) and (c)) cover higher excitation energy regions compared to the valence strengths. For example, the distribution of  $\ell = 0$  strength (see Fig. 10(a)) appears above 1 MeV, consistent with a tail of relatively weak strength from the shell above the valence orbitals. Similarly, much of the  $\ell = 2$  strength lies in many small fragments at higher excitations. There is some  $\ell = 2$  strength that appears



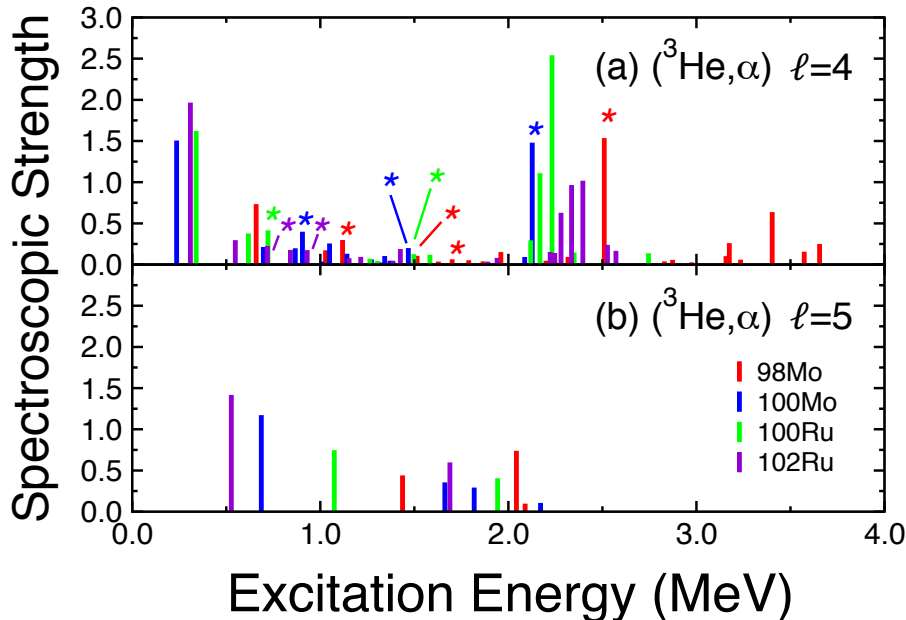


FIG. 7. (Color online) Distributions of the spectroscopic strength of states populated in  $(^3\text{He},\alpha)$  neutron transfer reaction on targets of  $^{102}\text{Ru}$  (violet),  $^{100}\text{Ru}$  (green),  $^{100}\text{Mo}$  (blue) and  $^{98}\text{Mo}$  (red) as a function of excitation energy for (a)  $\ell = 4$  and (b)  $\ell = 5$  transfers. The strength of individual states has been obtained from the measured cross sections using the DWBA reaction modeling and normalization procedures described in Section III. The asterisks indicate states with a  $J^\pi = 9/2^+$  assignment in the literature. Some states have been displaced slightly from their true excitation energy for clarity.

in a number of individual states at energies less than 1 MeV that have been interpreted previously by core-coupling [56] and Coriolis-coupling [57] models, where  $2d$  strength is brought down in excitation energy, with spectroscopic strengths similar to those observed here, by a mechanism somewhat analogous to the low-lying  $\ell = 3$  neutron strength discussed above.

Proton-removal reactions were not studied in the current work due to limitations in the available beam energy for  $(d,^3\text{He})$  reactions and difficulties with tritium handling for  $(t,\alpha)$  reactions. However limited information is available in the literature, albeit only on molybdenum isotopes, which can be used to assess the contributions to non-valence-shell orbitals in the ground states. A study of the  $(d,^3\text{He})$  reaction [58] has been performed and polarized  $(t,\alpha)$  data is reported in Ref. [59]. Neither reaction on  $^{98,100}\text{Mo}$  targets populated any  $\ell = 0$  strength. There are some inconsistencies between these two studies concerning  $\ell = 2$  strength, which are likely attributable to the lower resolution of the  $(d,^3\text{He})$  measurement. In  $^{97}\text{Nb}$ , the  $(d,^3\text{He})$  work observed states with  $\ell = 2$  strength at 1.764 and 2.090 MeV extracted by fitting several states to broad multiplet peaks; the  $(t,\alpha)$  study had higher resolution, made different assignments and reported no  $\ell = 2$  population in this nucleus. A state was observed at 0.817 MeV in both  $(d,^3\text{He})$  and  $(t,\alpha)$  reactions, the latter also populated states in  $^{99}\text{Nb}$  at 0.469 and 0.763 MeV, all with *tentative*  $\ell = 2$  assignments. Using the DWBA prescription presented below and cross section data from these references, the spectro-

scopic factors for the 0.469-, 0.763- and 0.817-keV states were estimated to be 0.09, 0.04 and 0.11. This allows us to estimate a limit for the occupation of  $\ell = 2$  in the ground state of  $^{99}\text{Nb}$  at the level of at most  $\sim 0.1$  protons.

### III. DWBA MODELING AND NORMALIZATION

Spectroscopic factors were deduced from the experimentally measured cross sections by comparison with the results of calculations using the distorted-wave Born approximation performed with the finite-range code PTOLEMY [60]. The optical potentials and bound states used in these calculations were chosen to be consistent with a recent global analysis of the quenching of spectroscopic strength [61] and are summarized below.

The form factors associated with the light-ion wave functions were taken from recent microscopic calculations. Those for the deuteron in  $(d,p)$  and  $(p,d)$  reactions were deduced using the Argonne  $v_{18}$  potential [62]. Recent Green's function Monte Carlo calculations provided form factors for  $A = 3$  and  $A = 4$  species [63].

The single-particle wave functions of the transferred particle in the heavy bound state were generated using a Woods-Saxon potential with fixed geometric parameters: radius parameter  $r_0 = 1.28$  fm and diffuseness  $a = 0.65$  fm. The depth was chosen to reproduce the measured binding energies. A spin-orbit component based on the derivative of a Woods-Saxon form with a

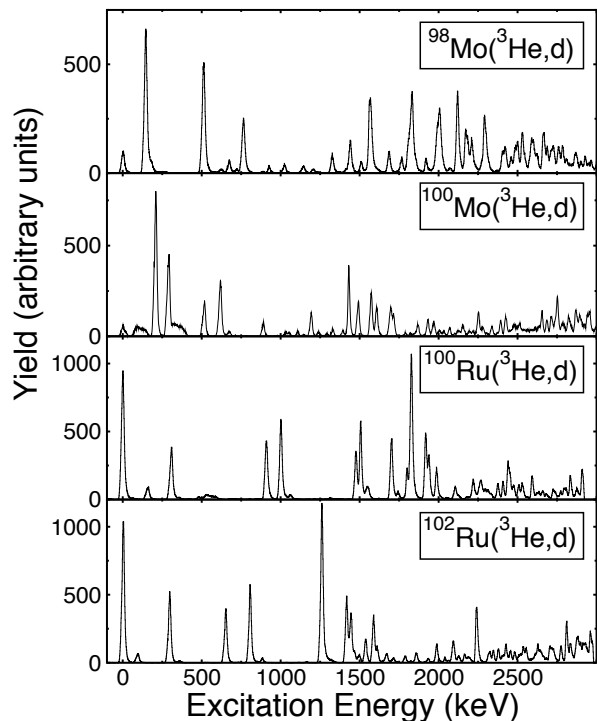


FIG. 8. Spectra of deuterons from the  $(^3\text{He},d)$  reaction on targets of  $^{98}\text{Mo}$ ,  $^{100}\text{Mo}$ ,  $^{100}\text{Ru}$  and  $^{102}\text{Ru}$  at a laboratory angle of  $6^\circ$  as a function of the excitation energy in the residual nucleus.

geometry defined by  $r_{\text{so}} = 1.10$  fm and  $a_{\text{so}} = 0.65$  fm, with a depth  $V_{\text{so}}$  of 6 MeV was used.

The distortions of incoming and outgoing partial waves were described using global optical-model potentials for protons, deuterons, helions and tritons taken from Refs. [64–66]. An  $\alpha$  potential deduced from elastic scattering in the  $A = 90$  region [67] was used.

In order to best satisfy the approximations of the DWBA approach, spectroscopic factors were deduced from cross sections at angles closest to the first peak of the angular distributions. In neutron transfer, the  $(d,p)$  and  $(p,d)$  reactions were used to determine spectroscopic strength for the lower orbital angular momentum transfer,  $\ell = 0$  and 2, and that for  $\ell = 4$  and 5 were deduced from  $(^3\text{He},\alpha)$  in order to ensure optimal momentum matching. The  $(^3\text{He},d)$  reaction is reasonably well-matched for all the relevant  $\ell$  in proton transfer.

The DWBA calculations used to extract spectroscopic factors from experimental cross sections carry an uncertainty in overall absolute normalization. Methods for determining the value of this normalization have been developed using the Macfarlane-French sum rules [68] that associate the summed spectroscopic strength to occupancies and vacancies of nucleon orbitals. Consistent results

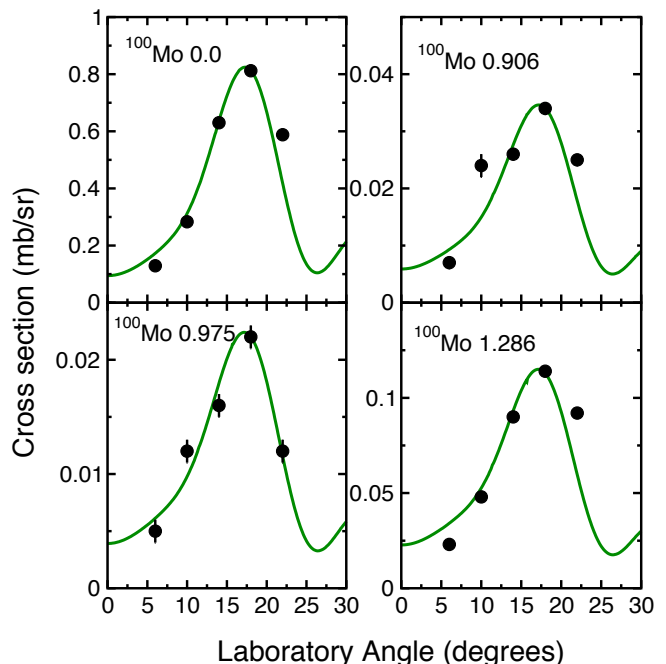


FIG. 9. (Color online) Examples of angular distributions for  $\ell = 4$  transitions assigned in the current work from the  $^{100}\text{Mo}(^3\text{He},d)$  reaction and for the previously assigned  $\ell = 4$  transition populating the residual ground state. The data are compared to the results of DWBA calculations using parameters listed in Section III for  $\ell = 4$ . The angular distributions are labelled by the target nucleus and the excitation energy in the residual system in units of MeV.

can be obtained by adopting a systematic approach to this process (see for example Ref. [53]). If the total low-lying strength is normalized to the full independent-particle value, the degree to which the resulting normalization factor deviates from unity is related to the quenching of single-particle strength that has been observed in other types of reactions such as  $(e, e'p)$ . Here we follow methods of Ref. [61] where a large-scale analysis resulted in normalization factors that were quantitatively consistent with previous measurements of such quenching.

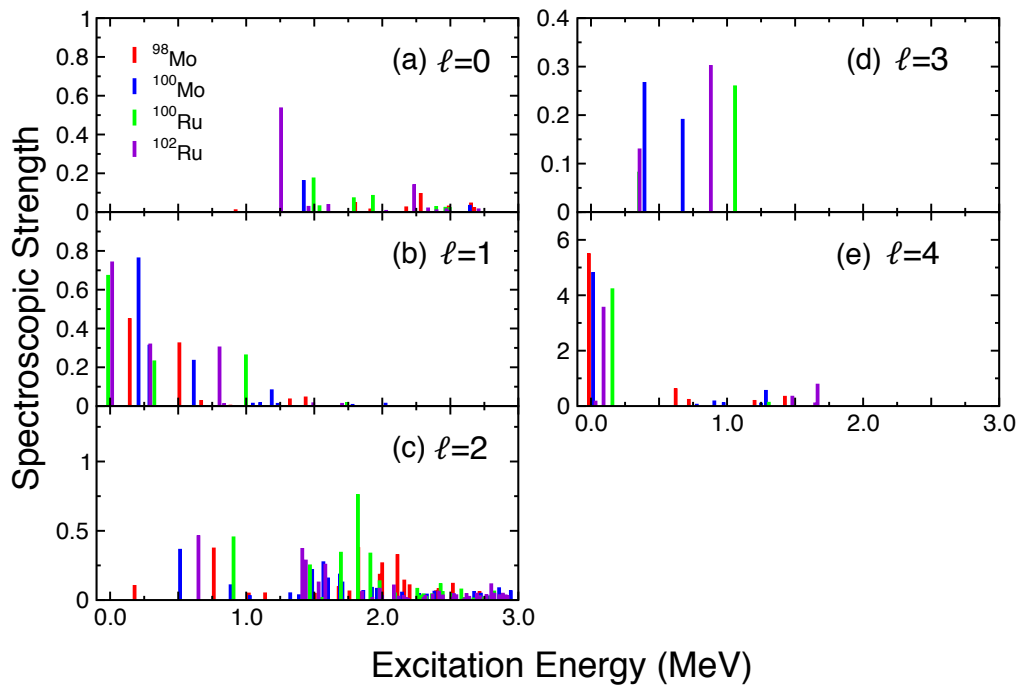


FIG. 10. (Color online) Distributions of the relative strength of proton states populated in the  $({}^3\text{He},d)$  reactions on targets of  ${}^{102}\text{Ru}$  (orange),  ${}^{100}\text{Ru}$  (green),  ${}^{100}\text{Mo}$  (red) and  ${}^{98}\text{Mo}$  (blue) as a function of excitation energy for (a)  $\ell = 0$ , (b)  $\ell = 1$ , (c)  $\ell = 2$ , (d)  $\ell = 3$  and (e)  $\ell = 4$  transitions. The relative strength of individual states has been obtained from the measured cross sections using the DWBA reaction modeling and normalization procedures described in Section III. The strength associated with the population of the ground states have been displaced in some cases slightly from 0 MeV for clarity.

TABLE II. Normalization factors for the DWBA calculations obtained using procedures described in the text.

	$(d,p)/(p,d)$ $\ell = 0$	$(d,p)/(p,d)$ $\ell = 2$	$({}^3\text{He},\alpha)$ $\ell = 4$ and 5	$({}^3\text{He},d)$
${}^{102}\text{Ru}$	0.642	0.673	0.570	0.682
${}^{100}\text{Ru}$	0.610	0.555	0.572	0.647
${}^{100}\text{Mo}$	0.624	0.617	0.576	0.639
${}^{98}\text{Mo}$	0.595	0.612	0.538	0.622
Mean	0.618	0.614	0.564	0.647
St Dev	0.020	0.048	0.018	0.025

For neutron-transfer reactions the following normalization procedure was adopted. The first step was to use the  $(d,p)$  and  $(p,d)$  data to deduce the summed spectroscopic strength for  $\ell = 0$  and 2, associated with the  $2s_{1/2}$  and  $1d$  orbitals. Via the sum rules [68], the summed strength for the neutron-adding reaction is proportional to the vacancy in the associated orbital. Similarly for the neutron-removing reaction, the summed strength is proportional to the occupancy. A DWBA normalization was chosen

such that the overall sum of strength from both neutron addition and removal gives the orbital degeneracy. Initially, this was done separately for both  $\ell = 0$  and 2 and for reactions on each target. The resulting normalization factors are shown in Table II. The average normalization across all targets for  $2s_{1/2}$  transfer was found to be 0.618 and that for the combined strengths associated with  $1d$  orbitals was 0.614. The individual normalization values varied across the targets used by 3% and 8% for  $\ell = 0$  and  $\ell = 2$  respectively. This variation, and that between the two  $\ell$  transfers, is small and so the overall average normalization constant of 0.616 was used in the subsequent analysis.

Assuming that the  $N = 50$  shell is closed, valence neutrons only occupy the  $2s_{1/2}$ ,  $1d$ ,  $0g_{7/2}$  and  $0h_{11/2}$  orbits (see comments above about the validity of this assumption). A normalization for the  $({}^3\text{He},\alpha)$  reaction was deduced by requiring that the sum of the previously normalised spectroscopic strength from  $(p,d)$  data for  $\ell = 0$  and 2 (i.e. the occupancy of those orbitals) and the spectroscopic strength for  $\ell = 4$  and 5 states from the  $({}^3\text{He},\alpha)$  reaction results in the expected total number of valence nucleons. The average normalization for  $\ell = 4$  and 5 transitions in the  $({}^3\text{He},\alpha)$  reaction was found to be 0.564, with a 3% variation across the four targets.

For proton transfer, a similar procedure was used where the total spectroscopic strength populated using the  $({}^3\text{He},d)$  reaction for all states corresponding to va-

lence protons was required to equal the expected number of proton vacancies in the  $Z = 50$  shell. The resulting normalization factor was 0.647 and the variation across targets was 4%.

A substantial set of transfer data was analyzed recently in a consistent fashion to determine the normalization of DWBA calculations and the associated quenching factor for single-particle motion in near-stable nuclei [61]. That analysis indicated that spectroscopic factors for a variety of light-ion induced transfer reactions across targets from  $^{16}\text{O}$  to  $^{208}\text{Pb}$  are quenched with respect to values from mean-field theory by a factor of 0.55, with a root-mean square spread of 0.1. This compares favorably with the normalization factors deduced in the current work. The consistency with independent data sets, along with the consistency across all four targets and between the different  $\ell$  values, gives confidence in the methodology used.

When considering isospin effects in the reactions, it should be noted that neutron adding and proton removal result in the population of states with a single value of isospin  $T + 1/2$ , where  $T$  is the isospin of the target. In contrast, in proton adding and neutron removal, states with both  $T + 1/2$  and  $T - 1/2$  are accessible. The set of states with higher isospin lie at higher excitation energies and are not observed in the kind of experiment described here. However, the summation in the Macfarlane and French sum rules should, in principle, contain strength associated with both values of isospin and the normalization procedure described above needs correcting for the unobserved strength. Using isospin symmetry, this could be done for proton-adding/neutron-removal reactions using spectroscopic strengths associated with the same orbitals populated in neutron-adding/proton-removal reactions [69]. However, protons and neutrons in these nuclei reside in different oscillator shells and the valence orbitals populated in neutron removal from all the target nuclei considered here are empty of protons. Subsequently, the required proton-removal strength is small. Given that the isospin Clebsch-Gordan coefficient is also small, the correction for the unobserved higher isospin is smaller still. Similarly for proton addition, the expectation is that the neutron-adding spectroscopic factors for  $g_{9/2}fp$  orbits would be small due to their high occupancy. Indeed, even if all the observed ( $d,p$ ) strength for  $\ell = 1, 3$  or  $4$  observed here were associated with the  $1p, 0f_{5/2}$  and  $0g_{9/2}$  orbitals, which is clearly a gross over-estimate, the normalization factors only change by a few percent. The isospin corrections were therefore considered small, compared to other uncertainties, in the current work and were not applied to the final analysis.

#### IV. NUCLEON OCCUPANCIES

Nucleon occupancies were deduced from summed spectroscopic strengths determined using the normalization factors described in the previous section. The neutron occupancies were extracted from the neutron-removing

reactions and are listed in Table III. Proton vacancies obtained from the ( $^3\text{He},d$ ) reaction are given in Table IV. These data are also shown graphically in Fig. 11. As noted above, the occupancy of non-valence orbitals in the ground states of these nuclei is estimated to be lower than 0.1 nucleons.

There are a number of systematic effects that could potentially influence the methodology adopted in deducing the nucleon occupancies. For example, it is well known that the results of DWBA calculations carry significant sensitivity to the input parameters used. The sensitivity of the current calculations was investigated using a variety of different optical-model potentials. Whilst the absolute values of the calculated cross sections varied considerably (by up to  $\sim 20\%$ ), the relative numbers relevant for the current analysis varied by up to 5%. Since statistical contributions are generally small, this is the largest contribution to the uncertainty in the deduced orbital occupancies and has been used as a basis to estimate the errors quoted in Tables III and IV; the high- $\ell$  neutron occupancies have an additional contribution discussed below. Using these estimates, the combined error on the total number of valence particles inferred from the experiment is typically  $\sim 0.2$ – $0.3$  depending on target. This is roughly consistent with the root-mean-square deviation of this number from the expected number of valence particles across the targets, 0.1 for neutrons and 0.2 for proton holes. These error estimates are also similar to those obtained in occupancy measurements of other nuclear systems [5, 6, 9–11].

Beyond direct nucleon transfer, there are other more complicated reaction mechanisms that can contribute to the measured yields. Recent transfer work on nickel isotopes [53] presented a method to estimate the contribution of multistep processes by comparing the spectroscopic strength of states populated by a well-matched and a poorly-matched reaction. This was applied to  $\ell = 4$  transitions in the current data set populated by the ( $p,d$ ) and ( $^3\text{He},\alpha$ ) reactions and gave a very similar estimate to that in Ref. [53]. Multistep processes are estimated to contribute at a level of around  $0.002(2j + 1)$  in the spectroscopic strength of states deduced using a reaction with good matching. Most of the strength contributing to the sum-rule analysis is from states populated much more strongly than this level and therefore multistep processes appear not to influence the data strongly.

There are a few influences associated with spin assignments that could affect the deduced occupancies. The most important of these is the assignment of the spins of states populated via  $\ell = 4$  transfer in neutron-removal reactions. As noted above, a choice was made to associate all  $\ell = 4$  strength below 2 MeV with the  $0g_{7/2}$  orbital unless it had a previous  $9/2^+$  assignment, but other approaches could be adopted. For example, one could use only the strength associated with states with a previous  $7/2^+$  assignment. If this were done, the  $0g_{7/2}$  occupancies in the  $A = 100$  isotopes change by  $\sim 0.1$  neutrons due to changes in the summed  $\ell = 4$  strength in those

TABLE III. Experimental neutron occupancies determined from neutron-removing reactions. The difference between the summed occupancy and the expected number of valence neutrons is also given. The decreases in neutron occupancies of each orbital associated with double  $\beta$  decay of  $^{100}\text{Mo}$  are given at the bottom of the table. The errors quoted are based on relative variations due to choices of potentials in the DWBA and, in the case of high- $\ell$  orbitals, a contribution to reflect a systematic effect from spin assignment for  $\ell = 4$  (see text for details).

	$2s_{1/2}$	$1d$	$0g_{7/2}$	$0h_{11/2}$	Total	Expected	Difference
$^{102}\text{Ru}$	0.29(1)	2.89(14)	2.88(38)	2.00(14)	8.05(43)	8	0.05
$^{100}\text{Ru}$	0.23(1)	2.50(12)	2.19(15)	1.13(8)	6.05(21)	6	0.05
$^{100}\text{Mo}$	0.33(2)	3.40(17)	2.48(19)	1.89(13)	8.09(29)	8	0.09
$^{98}\text{Mo}$	0.17(1)	3.34(17)	1.13(6)	1.25(9)	5.88(20)	6	-0.12
$^{100}\text{Mo-Ru}$	0.09(2)	0.90(21)	0.30(24)	0.76(15)	2.05(36)		

TABLE IV. Experimental proton vacancies determined from the ( $^3\text{He},d$ ) reaction. The difference between the summed vacancy and the expected number of valence proton holes is also given. The increases in proton occupancy in each orbital associated with double  $\beta$  decay of  $^{100}\text{Mo}$  are also given at the bottom of the table. The errors quoted are based on relative variations due to choices of potentials in the DWBA (see text for details).

	$1p$	$0f_{5/2}$	$0g_{9/2}$	Total	Expected	Difference
$^{102}\text{Ru}$	1.43(7)	0.90(5)	3.98(20)	6.32(22)	6	0.32
$^{100}\text{Ru}$	1.21(6)	0.35(2)	4.44(22)	6.00(23)	6	0.00
$^{100}\text{Mo}$	1.49(7)	0.47(2)	5.94(30)	7.89(31)	8	-0.11
$^{98}\text{Mo}$	0.91(5)	–	6.78(34)	7.69(34)	8	-0.31
$^{100}\text{Mo-Ru}$	0.28(10)	0.12(3)	1.50(37)	1.90(38)		

nuclei, with a smaller 5% decrease in  $\ell = 5$  occupancies due to the associated shift in the ( $^3\text{He},\alpha$ ) normalization. However, the consistency in the individual normalization factors is then worse than in the adopted approach, probably reflecting variation in the extent of  $J^\pi$  assignments for the residual nucleus in the literature. These effects have been added in quadrature to the errors for  $\ell = 4$  and 5 orbitals in Table III as an estimate of this systematic effect. Variation in the excitation-energy limit used to exclude the higher-lying  $0g_{9/2}$  strength has less consequence.

In addition, there are a number of states observed in the ( $^3\text{He},\alpha$ ) reaction that are not obviously populated in the ( $p,d$ ) reaction; these are candidates for  $\ell = 4$  or 5 transitions, but the lack of ( $p,d$ ) data makes assignment difficult and they have not been included in the analysis. If they were introduced, the *maximum* effect they make for the occupancies of the high- $\ell$  neutron orbitals is 0.1 nucleons. Other minor complications, such as tentative assignments and unresolved doublets, affect the final results at a much lower level.

## V. DISCUSSION

The measured neutron occupancies shown in Fig. 11 indicate that neutrons occupy each of the orbitals in the shell above  $N = 50$ , with the different  $\ell$  values full to at least 10% of the maximum occupancy. Although the current measurements cannot distinguish between the two  $1d$  orbitals, much of the  $\ell = 2$  strength populated here is associated with states that have a  $J^\pi$  assignment in the literature (as summarized in Refs. [49–52] and references therein). The fraction of  $\ell = 2$  strength without a  $J^\pi$  assignment varies from  $\sim 10$  to 25% across the different targets. Using the known  $J^\pi = 5/2^+$  strength, a lower limit on the occupancy of the  $1d_{5/2}$  orbital is estimated as 1.8, 1.9, 2.4 and 3.0 neutrons in  $^{102,100}\text{Ru}$  and  $^{100,98}\text{Mo}$  respectively, indicating that this orbital is responsible for most of the observed  $1d$  occupancy.

The proton Fermi surface lies below  $Z = 50$ . The pattern of proton vacancy is shown in Fig. 11, and illustrates that the  $0f_{5/2}$  orbital is almost full and the  $1p$  orbitals carry around two thirds of their maximum occupancy, whereas the  $0g_{9/2}$  state is only partially occupied. For the  $\ell = 1$  strength, at least 90% of the states populated on each target have a  $J^\pi$  assignment in the literature

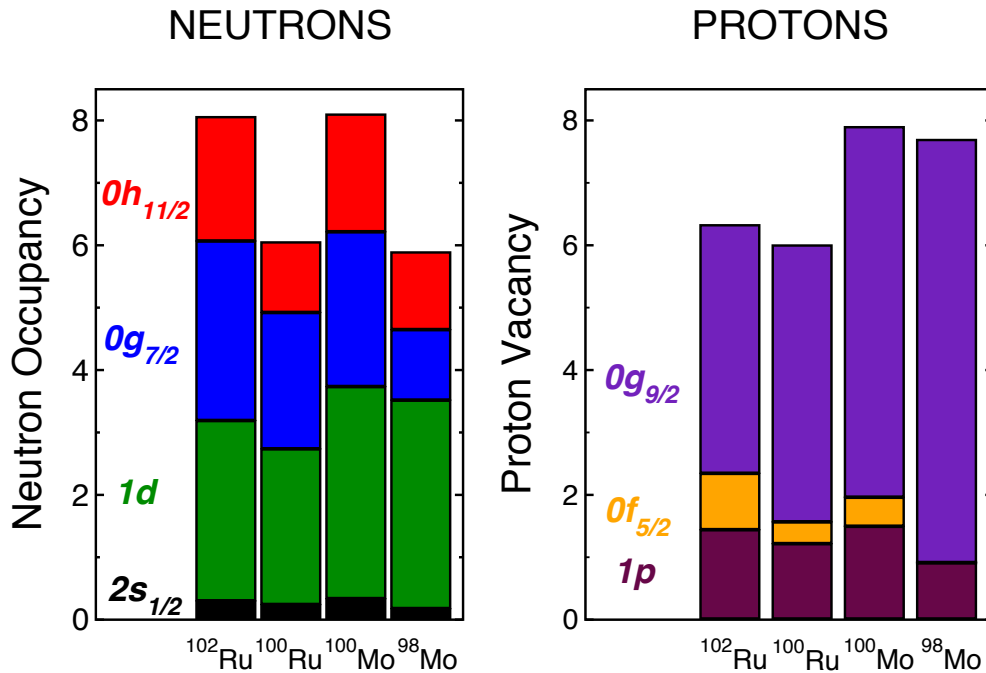


FIG. 11. (Color online) Experimentally determined neutron occupancies and proton vacancies for the valence orbits in  $^{100}\text{Mo}$  and  $^{100}\text{Ru}$ , along with  $^{102}\text{Ru}$  and  $^{98}\text{Mo}$  which are used for consistency checks.

([49–52] and references therein). Applying these  $J^\pi$  assignments suggests that the  $1p_{3/2}$  orbital has a vacancy of at most 14% across the different targets, with the  $1p_{1/2}$  orbital empty to the level of at most 39%. Given the vacancy in the  $1p$  orbitals, it would appear from these results that the  $Z = 40$  sub-shell closure, assumed in some shell-model calculations, is somewhat weak in these systems.

The comparison of measured nucleon occupancies with those extracted from theoretical studies of nuclear matrix elements for double  $\beta$  decay has proved very instructive in the past, as illustrated by the example of Ref. [7] in the case of  $^{76}\text{Ge}$  decay. However, quantitative occupancy numbers are not always given in theoretical publications. The  $^{100}\text{Mo}$ – $^{100}\text{Ru}$  system has been the subject of several theoretical determinations of the nuclear matrix element for  $0\nu 2\beta$  decay and associated orbital occupancies are available for calculations using the interacting boson model (IBM) and quasi-particle random-phase approximation (QRPA). Nucleon occupancies can be extracted from the IBM wave functions relatively easily as discussed in Ref. [72]. QRPA calculations take as input single-particle energies and occupancies, often from BCS calculations using a Woods-Saxon potential (WS). Whilst it is easy to use such inputs to compare with measured occupancies, it would be more consistent to compare the current results with the occupancies contained

in the correlated QRPA ground states. This results in complications as standard QRPA methods do not automatically conserve particle number, even on average. Reformulations of QRPA methods that ensure average particle number conservation do exist; for example, the self-consistent renormalised approach (SRQRPA) taken in Ref. [7] has been applied to the  $^{76}\text{Ge}$   $0\nu 2\beta$  decay system. There are differences in occupancies predicted by the BCS approximation and SRQRPA, but these tend to be small except for some orbitals with higher orbital angular momentum [73]. Since, to the best of our knowledge, SRQRPA calculations have not been done for the  $A = 100$  system, here we will compare with the available occupancies used as inputs to QRPA calculations and note this issue for future theoretical attention.

Valence neutron occupancies and proton vacancies are shown in Fig. 12 compared to IBM and WS calculations. Two sets of results for the Woods-Saxon potential are shown; one taken from a standard parameterization adopted near the line of stability [74] (labeled WS in Fig. 12) and one (labeled WS ADJ in Fig. 12) after adjustments to better reproduce quasi-particle states in nearby odd- $A$  nuclei (see Ref. [73] and references therein for details). This set has been used as input not only to calculations of both single EC, single  $\beta$  and two-neutrino double  $\beta$  decays [73, 75], but has also been used for  $0\nu 2\beta$  decay [75, 76].

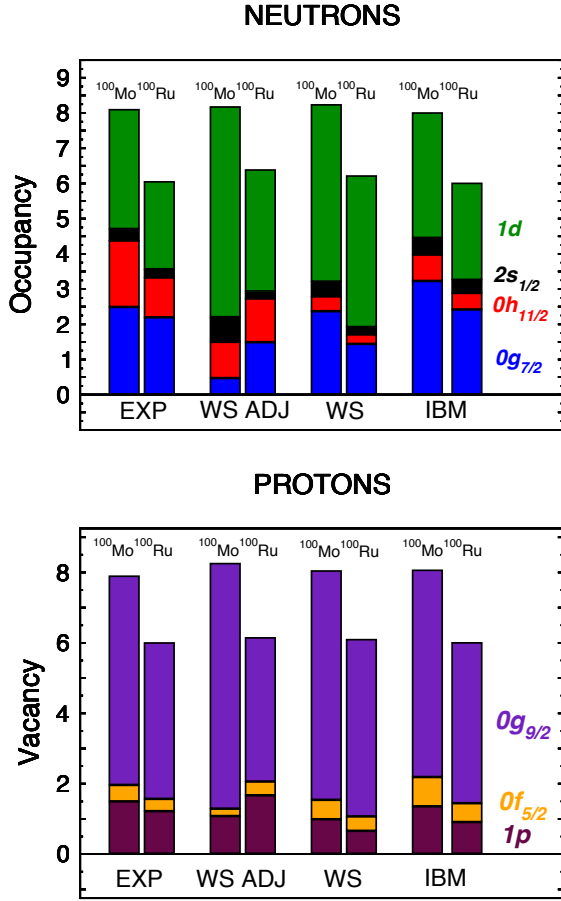


FIG. 12. (Color online) Experimentally determined neutron occupancy and proton vacancy for the valence orbits in  $^{100}\text{Mo}$  and  $^{100}\text{Ru}$  compared to those predicted by the interacting boson model (IBM) [71, 72] and two different Woods-Saxon calculations [73, 74].

For protons, most of these calculations appear to give a reasonable overall description of the measured vacancies. For the IBM calculations, the discrepancies are at the level of a couple of tenths of a nucleon and probably within the uncertainties in the experiments. For the WS results, the overall picture is similar, but discrepancies are slightly larger. However, in the case of the adjusted Woods-Saxon calculations, the comparison with the experimental vacancies is worse than the other calculations, particularly for  $^{100}\text{Mo}$  where there is significant over prediction of the vacancy of the  $0g_{9/2}$  orbital.

For neutrons, the comparisons are more mixed. The IBM calculations appear to slightly overestimate the neutron occupancy of the positive-parity orbitals at the expense of the  $0h_{11/2}$  orbit, which is predicted to have significantly lower occupation than the current data suggests. The underestimation of the occupancy of this intruder orbit persists in the WS calculations, but results in over prediction for  $1d$  neutrons. The adjusted WS calculations do have a better reproduction of the experimental

$0h_{11/2}$  occupancy, but fail to reproduce the numbers of neutrons in the  $1d$  and  $0g_{9/2}$  orbitals; these discrepancies appear to be more dramatic in the case of  $^{100}\text{Mo}$ . The larger discrepancies referred to here are significant compared to the experimental uncertainties, accompanied by less significant issues with  $2s_{1/2}$  neutrons. None of the calculations fare as well with the neutron occupancies as they do with the predictions of the arrangement of protons in the valence orbits.

The changes in nucleon occupancies during a potential double  $\beta$  decay of  $^{100}\text{Mo}$  are also given in the Tables III and IV and displayed graphically in Fig. 13. For convenience, changes in the numbers of neutrons and protons are both quoted as positive numbers and therefore indicate the number of neutrons lost and the number of protons gained in the decay process. The neutron occupancy measurements indicate that the  $1d$  (mainly the  $j = 5/2$  spin-orbit partner, assuming estimates above using existing assignments are correct) and  $0h_{11/2}$  orbits participate strongly in a double  $\beta$  decay process between the ground states of the parent and daughter. There are smaller contributions from the  $2s_{1/2}$  and  $0g_{7/2}$  orbitals. The number of protons increases during the decay mainly in the  $0g_{9/2}$  orbital, with the  $1p$  protons (presumably with  $j = 1/2$ ) playing a lesser role and a much smaller contribution from the  $0f_{5/2}$  orbital.

Since the distribution of protons amongst the valence orbitals in the parent and daughter nuclei are fairly well reproduced in the WS and IBM calculations, the picture of rearrangements of protons in such a decay are also reasonably well predicted overall, with some small differences in the contributions from different proton orbits as shown in Fig. 13. The adjusted Woods-Saxon results appear to exaggerate the rearrangement of protons during a decay; increases in  $0g_{9/2}$  occupancy by more than two protons is compensated by depletion of proton  $0f_{5/2}$  and  $1p$  orbitals. Similarly, in the same calculation, more than two neutrons disappear from the  $2s_{1/2}$  and  $1d$  orbitals, balanced by increases in the  $0h_{11/2}$  and  $0g_{7/2}$  neutron occupancy. Such dramatic rearrangements are not substantiated in the experimental measurements for either type of nucleon. The predicted neutron occupancy changes in the WS and IBM calculations are rather similar to one another and to the experimental results for  $2s_{1/2}$  and  $1d$  neutrons, but the observed balance of neutron  $0h_{11/2}$  and  $0g_{7/2}$  contributions to the decay is not well reproduced.

None of the theoretical descriptions presented here reproduce all of the orbital occupancies and nucleon rearrangements, deduced from the current experimental work, that would occur during the double  $\beta$  decay of  $^{100}\text{Mo}$ . The effect of the discrepancies on decay probability is somewhat difficult to judge without further theoretical investigation. Certainly the dramatic rearrangement of nucleons implicit in the adjusted Woods-Saxon calculations, which naively might hinder a decay, seem unwarranted by the current results. These appear to arise mostly from problems with the adjustments made in the

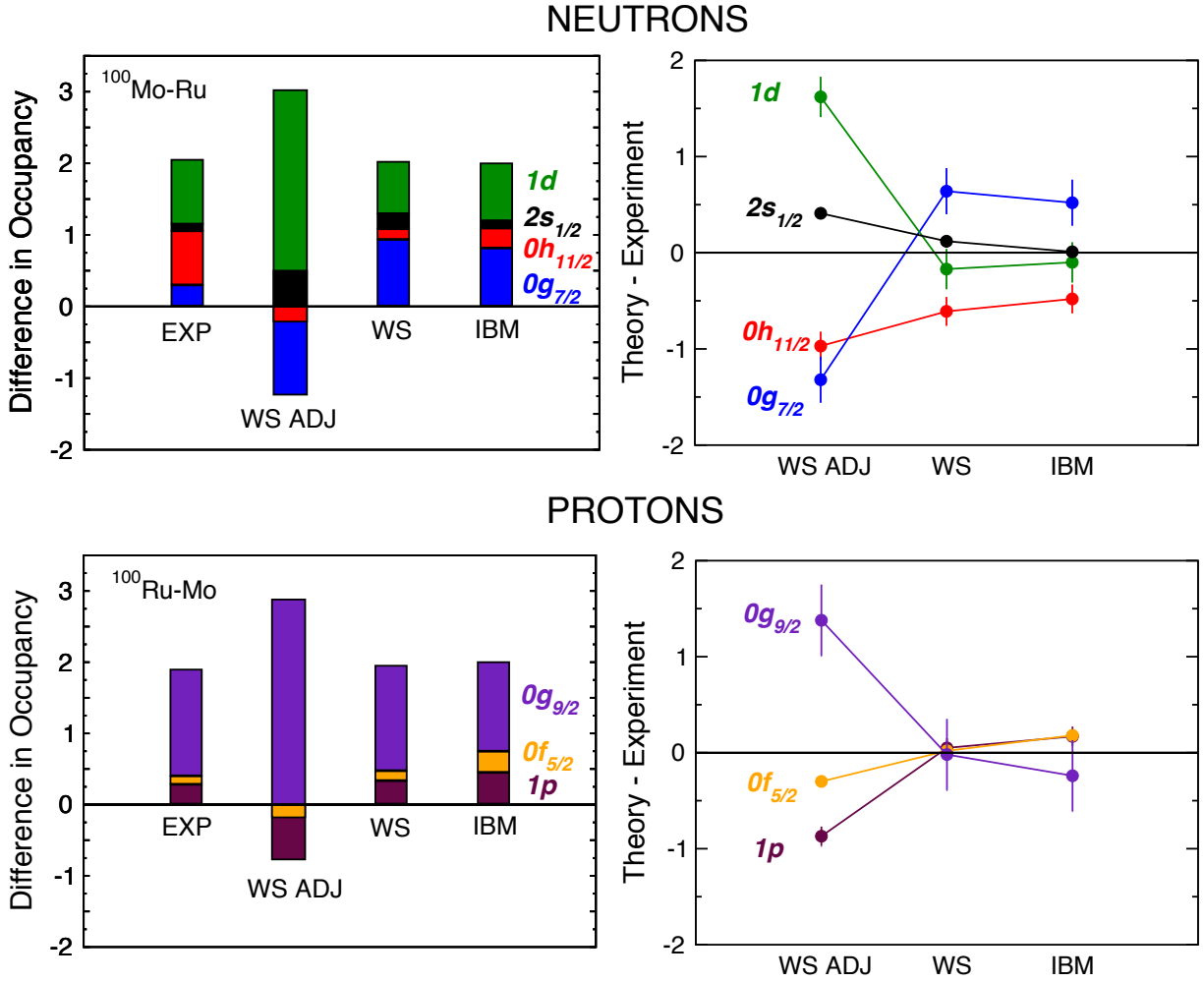


FIG. 13. (Color online) Left: Changes in the occupancy of valence nucleon orbitals during a double  $\beta$  decay of  $^{100}\text{Mo}$  deduced from experimentally measured occupancies (EXP) compared to those predicted by a number of different theoretical calculations of double  $\beta$  decay where the the same labeling as Fig. 12 has been used (see text for details). The signs are chosen such that a reduction in the number of neutrons and a gain in the number of protons are positive numbers. Right: The difference between the theoretical calculations and experimental numbers plotted with experimental errors.

case of  $^{100}\text{Mo}$ . Indeed, the data presented here and in the Supplemental Material [46] for single-particle excitations in odd-A nuclei form a good basis on which to reassess the adjustments associated with both  $^{100}\text{Mo}$  and  $^{100}\text{Ru}$ , with additional constraining data for the other nuclei populated in the current work on  $^{98}\text{Mo}$  and  $^{102}\text{Ru}$  targets. While the IBM and unadjusted WS models seem to give a reasonable overall picture for protons, significant differences arise for the predicted neutron occupancies and rearrangements, particularly for the higher- $\ell$  orbits. It may prove instructive to determine the quantitative effect on the nuclear matrix element for  $0\nu 2\beta$  decay if these theoretical approaches were adjusted to more accurately reproduce the measured occupancies and also to extract theoretical occupancies at the QRPA level to refine the comparison with data presented here.

## VI. CONCLUSION

We report on an experimental determination of neutron occupancies and proton vacancies from data on the  $(d,p)$ ,  $(p,d)$ ,  $(^3\text{He},\alpha)$  and  $(^3\text{He},d)$  reactions on  $^{98,100}\text{Mo}$  and  $^{100,102}\text{Ru}$  isotopes. The work provides a detailed quantitative assessment of the rearrangements of protons and neutrons amongst the valence single-particle orbitals during double  $\beta$  decay of  $^{100}\text{Mo}$ . There are significant disagreements with theoretical calculations of the same properties, calculations which have also been used to determine the nuclear matrix element for  $0\nu 2\beta$  decay. We hope that these data will stimulate further theoretical attention to refine future calculations of this quantity, which could be a critical component in developing our understanding of the properties of neutrinos should the rare process of  $0\nu 2\beta$  decay ever be



observed.

## VII. ACKNOWLEDGMENTS

We would like to acknowledge the accelerator operating staff and target makers at the Maier-Leibnitz Laboratorium der Münchner Universitäten. This material is based upon work supported by the UK Science and Technology Facilities Council, the US Department of Energy, Office of Nuclear Physics, under Contract No. DE-AC02-06CH11357, the National Science Foundation Grant No. PHY-08022648 (JINA) and the DFG Cluster of Excellence “Origin and Structure of the Universe”.

- 
- [1] Petr Vogel, *J. Phys. G* **39**, 124002 (2012).
- [2] J. Kotila and F. Iachello, *Phys. Rev. C* **87**, 024313 (2013).
- [3] J.N. Bahcall, H. Murayama, and C. Peña-Garay, *Phys. Rev. D* **70**, 033012 (2004).
- [4] S.J. Freeman and J.P. Schiffer, *J. Phys. G* **39**, 124004 (2012).
- [5] J. P. Schiffer, S. J. Freeman, J. A. Clark, C. Deibel, C.R. Fitzpatrick, S. Gros, A. Heinz, D. Hirata, C.L. Jiang, B.P. Kay, A. Parikh, P.D. Parker, K.E. Rehm, A.C.C. Villari, V. Werner, and C. Wrede, *Phys. Rev. Lett.* **100**, 112501 (2008).
- [6] B.P. Kay, J.P. Schiffer, S.J. Freeman, T. Adachi, J.A. Clark, C.M. Deibel, H. Fujita, Y. Fujita, P. Grabmayr, K. Hatanaka, D. Ishikawa, H. Matsubara, Y. Meada, H. Okamura, K.E. Rehm, Y. Sakemi, Y. Shimizu, H. Shimoda, K. Suda, Y. Tameshige, A. Tamii, and C. Wrede, *Phys. Rev. C* **79**, 021301(R)(2009).
- [7] Fedor Šimkovic, Amand Faessler, and Petr Vogel, *Phys. Rev. C* **79**, 015502 (2009).
- [8] J. Menéndez, A. Poves, E. Caurier, and F. Nowacki, *Phys. Rev. C* **80**, 048501 (2009).
- [9] B.P. Kay, T. Bloxham, S.A. McAllister, J.A. Clark, C.M. Deibel, S.J. Freedman, S.J. Freeman, K. Han, A.M. Howard, A.J. Mitchell, P.D. Parker, J.P. Schiffer, D.K. Sharp, and J.S. Thomas, *Phys. Rev. C* **87**, 011302(R)(2013).
- [10] J. P. Entwisle, B. P. Kay, A. Tamii, S. Adachi, N. Aoi, J. A. Clark, S. J. Freeman, H. Fujita, Y. Fujita, T. Furuno, T. Hashimoto, C. R. Hoffman, E. Ideguchi, T. Ito, C. Iwamoto, T. Kawabata, B. Liu, M. Miura, H. J. Ong, J. P. Schiffer, D. K. Sharp, G. Süsoy, T. Suzuki, S. V. Szewc, M. Takaki, M. Tsumura, and T. Yamamoto *Phys. Rev. C* **93**, 064312 (2016).
- [11] S. V. Szewc, B. P. Kay, T. E. Cocolios, J. P. Entwisle, S. J. Freeman, L. P. Gaffney, V. Guimarães, F. Hammache, P. P. McKee, E. Parr, C. Portail, J. P. Schiffer, N. de Séréville, D. K. Sharp, J. F. Smith, and I. Stefan *Phys. Rev. C* **94**, 054314 (2016).
- [12] J.S. Thomas, S. J. Freeman, C.M. Deibel, T. Faestermann, R. Hertenberger, B. P. Kay, S. A. McAllister, A. J. Mitchell, J. P. Schiffer, D.K. Sharp and H.-F. Wirth, *Phys. Rev. C* **86**, 047304 (2012).
- [13] R. Arnold et al., *Phys. Rev. D* **89**, 11101 (2014).
- [14] R. Arnold et al., *Phys. Rev. D* **92**, 072011 (2014).
- [15] H. Bhang et al., *Journal of Physics: Conference Series* **375** (2012) 042023.
- [16] A. S. Barabash, D. M. Chernyak, F. A. Danevich, A. Giuliani, I. M. Ivanov, E. P. Makarov, M. Mancuso, S. Marnieros, S. G. Nasonov, C. Nones, E. Olivieri, G. Pessina, D. V. Poda, V. N. Shlegel, M. Tenconi, V. I. Tretiyak, Ya. V. Vasiliev, M. Velazquez, V. N. Zhdankov, *Eur. Phys. J. C* **74** 3133 (2014).
- [17] Sven A.E. Johansson *Nuclear Physics* **64**, 147 (1965).
- [18] A.G. Smith, J.L. Durell, W.R. Phillips, W. Urban, P. Sarriguren, and I. Ahmad, *Phys. Rev. C* **86**, 014321 (2012).
- [19] F.C. Charlwood, K. Baczynska, J. Billowes, P. Campbell, B. Cheal, T. Eronen, D.H. Forest, A. Jokinen, T. Kessler, I.D. Moore, H. Penttilä, R. Powis, M. Ruffer, A. Saastamoinen, G. Tungate, J. Äystö, *Physics Letters B* **674** (2009) 2327.
- [20] W.H. King, *Proc R Soc A* **280** (1964) 430.
- [21] J.A. Shannon, W.R. Phillips, J.L. Durell, B.J. Varley, W. Urban, C.J. Pearson, I. Ahmad, C.J. Lister, L.R. Morss, K.L. Nash, C.W. Williams, N. Schulz, E. Lubluewicz and M. Bentaleb, *Physics Letters B* **336** (1994) 136.
- [22] E. E. Habib, J. A. Cameron, G. U. Din, V. Janzen, and R. Schubank, *Phys. Rev. C* **26**, 834 (1982).
- [23] E. E. Habib, J. A. Cameron, G. U. Din, V. Janzen, and R. Schubank, *Can. J. Phys.* **68**, 1332 (1990).
- [24] Helmuth Seyfarth, Hasan H. Güven, Bela Kardon, Gérard Lhersonneau, Kornel Sistemich, Slobodan Brant, Norbert Kaffrell, Peter Maier-Komor, Helbert K. Vonach, Vlandimir Paar, Dražen Vorkapić, Richard A. Meyer, *Fizika (Zagreb)* **22**, 183 (1990).
- [25] W. Booth, S.M. Dalglish, K.C. McLean, R.N. Glover and F.R. Hudson, *Phys. Lett. B* **30**, 335 (1969).
- [26] W. L. Sievers, D. A. Close, C. J. Umbarger, R. C. Bearse, and F. W. Prosser, Jr., *Phys. Rev. C* **6**, 1001 (1972).
- [27] Sven A. Hjorth and Bernard L. Cohen, *Phys. Rev.* **135**, B920 (1964).
- [28] P. K. Bindal, D. H. Youngblood, R. L. Kozub, and P. H. Hoffmann-Pinther, *Phys. Rev. C* **12**, 1826 (1975).
- [29] S. Hirowatari, Syafarudin, F. Aramaki, A. Nohtomi, G. Wakabayashi, Y. Uozumi, N. Ikeda, M. Matoba, Y. Aoki, K. Hirota, N. Okumura, and T. Joh, *Nuc. Phys. A* **714**, 3 (2003).
- [30] T. Ishimatsu, S. Hayashibe, N. Kawamura, T. Awaya, H. Ohmura, Y. Nakajima, and S. Mitarai, *Nucl. Phys. A* **185**, 273 (1972).
- [31] Toshiyuki Ishimatsu, Shogo Hayashibe, Takashi Awaya, and Haruko Ohmura. *J. Phys. Soc. Jap.* **35**, 1579 (1973).

- [32] J. B. Moorhead and R. A. Moyer, *Phys. Rev.* **184**, 1205 (1969).
- [33] W. Dietrich, G. Ch. Madueme, L. Westerberg and A. Bäcklin, *Phys. Scripta* **12**, 271 (1975).
- [34] P. K. Bindal, D. H. Youngblood, R. L. Kozub, and P. H. Hoffmann-Pinther, *Phys. Rev. C* **12**, 390 (1975).
- [35] H. T. Fortune, G. C. Morrison, J. A. Nolen, Jr., and P. Kienle, *Phys. Rev. C* **3**, 337 (1971).
- [36] G.P.A. Berg, M. Demarteau, A. Hardt, W. Hürlimann, S.A. Martin, J. Meissburger, W. Oelert, H. Seyfarth, B. Styczen, M. Köhler, I. Oelrich, and J. Scheerer, *Nucl. Phys. A* **379**, 93 (1982).
- [37] M. D. L. Barbosa, T. Borello-Lewin, L. B. Horodyski-Matsushigue, J. L. M. Duarte, G. M. Ukita, and L. C. Gomes, *Phys. Rev. C* **58**, 2689 (1998).
- [38] A. Mito, K. Komura, T. Mitsugashira, and K. Otozai, *Nucl. Phys. A* **129**, 165 (1969).
- [39] S A Dickey, J J Kraushaar, and M A Rumore, *J. Phys. G.* **12**, 745 (1986).
- [40] J. L. M. Duarte, L. B. Horodyski-Matsushigue, T. Borello-Lewin, and O. Dietzsch, *Phys. Rev. C* **38**, 664 (1988).
- [41] C.L. Hollas, K.A. Aniol, D.W. Gebbie, M. Borsaru, J. Nurzynski, and L.O. Barbopoulos, *Nucl. Phys. A* **276**, 1 (1977).
- [42] J. Schoonover, H.C. Cheung, J.E. Kitching, S.K. Mark, and J. K. P. Lee, *Z. Phys. A* **272**, 99 (1975).
- [43] H.C. Cheung, S.I. Hayakawa, J.E. Kitching, J. K. P. Lee, S.K. Mark and J. C. Waddington, *Z. Phys. A* **280**, 149 (1977).
- [44] R.J. Peterson, R.A. Emigh, and R.E. Anderson, *Nucl. Phys. A* **290**, 155 (1977).
- [45] H C Cheung, J Kitching, J K P Lee, and S K Mark, *J. Phys. G.* **1**, 737 (1975).
- [46] See Supplemental Material [URL will be inserted by publisher] for cross sections and spectroscopic factors associated with individual states.
- [47] H.J. Scheerer, H. Vonach, M. Löffler, A.v.d. Decken, M. Goldschmidt, C.A. Wiedner H.A. Enge, *Nucl. Instru. Methods* **136**, 213 (1976)
- [48] H.-F. Wirth, Ph.D. Thesis, Technische Universität München 2001 (unpublished).
- [49] E. Browne and J. K. Tuli, *Nuclear Data Sheets* **112**, 275 (2011).
- [50] N. Nica, *Nuclear Data Sheets* **111**, 525 (2010).
- [51] Jean Blachot, Evaluated Nuclear Structure Data File for  $A = 101$  compiled 1-Jul-2006 <http://www.nndc.bnl.gov/>
- [52] D. De Frenne, *Nuclear Data Sheets* **110**, 2081 (2009).
- [53] J.P. Schiffer, C.R. Hoffman, B.P. Kay, J.A. Clark, C.M Deibel, S.J. Freeman, A.M Howard, A.J. Mitchell, P.D. Parker, D.K. Sharp and J.S. Thomas. *Phys. Rev. Lett.* **108** 022501 (2012).
- [54] S.E. Vigdor and W.Haerberli *Nucl.Phys. A* **253**, 55 (1975).
- [55] J. L. M. Duarte, T. Borello-Lewin and L. B. Horodyski-Matsushigue, *Phys. Rev. C* **50**, 666 (1994).
- [56] P.K. Bindal and D.H. Youngblood, *Phys. Rev. C* **9** 1618, (1974).
- [57] Å Bredbacker, M. Brenner and F.B. Malik, *Nucl. Phys. A* **253**, 55 (1975).
- [58] P.K. Bindal, D.H. Youngblood and R.L. Kozub, *Phys. Rev. C* **10** 729, (1974).
- [59] E.R. Flynn, Ronald E. Brown, F. Ajzenberg-Selove, and J.A. Cizewski *Phys. Rev. C* **28** 575, (1983).
- [60] M. H. Macfarlane and S. C. Pieper, ANL-76-11 Rev. 1, ANL Report (1978).
- [61] B.P. Kay, J.P. Schiffer and S.J. Freeman, *Phys. Rev. Lett.* **111** 042502 (2013).
- [62] R.B. Wiringa, V.G.J Stoks and R. Schiavilla, *Phys. Rev. C* **51** 38, (1995).
- [63] I. Brida, S.C. Pieper and R.B. Wiringa, *Phys. Rev. C* **84** 024319, (2011).
- [64] A.J. Koning and J.P. Delaroche, *Nucl. Phys. A* **713**, 231 (2003).
- [65] H. An and C. Cai, *Phys. Rev. C* **73** 054605, (2006).
- [66] D.Y. Pang, P. Roussel-Chomaz, H. Savajols, R.L. Varner and R. Wolski, *Phys. Rev. C* **79** 024615, (2009).
- [67] G. Bassani and J Picard, *Nucl. Phys. A* **131**, 653 (1969).
- [68] M. H. Macfarlane and J. B. French, *Rev. Mod. Phys.* **32**, 567 (1960).
- [69] J.P. Schiffer, Chapter 13 Isospin in Transfer Reactions, in *Isospin in Nuclear Physics*, edited by D.H. Wilkinson (Elsevier 1969).
- [70] R. C. Johnson and P. C. Tandy, *Nucl. Phys. A* **235**, 56 (1974).
- [71] J. Kotila (private communication).
- [72] J. Kotila and J. Barea, *Phys. Rev. C* **94**, 034320 (2016).
- [73] J. Suhonen and O. Civitarese, *Nucl. Phys. A* **924**, 1 (2014).
- [74] J. Suhonen (private communication).
- [75] Jouni Suhonen, *Nucl. Phys. A* **700**, 649 (2002).
- [76] J. Suhonen and O. Civitarese, *Phys. Rev. C* **49**, 3055 (1994).